Paleobiology, 36(4), 2010, pp. 555–572

Shape analysis of filamentous Precambrian microfossils and modern cyanobacteria

David Boal and Ray Ng

Abstract.—Variations in the orientation and cross-sectional shape of filamentous microfossils provide quantitative measures for characterizing them and probing their native mechanical structure. Here, we determine the tangent correlation length, which is the characteristic length scale for the variation in direction of a sinuous curve, for both a suite of Precambrian filamentous microfossils and six strains of modern filamentous cyanobacteria, all with diameters of a few microns. Among 1.9–2-Ga microfossils, *Gunflintia grandis*, *Gunflintia minuta* and *Eomycetopsis filiformis* possess, respectively, correlation lengths of 360 ± 40 μm, 670 ± 40 μm and 700 ± 100 μm in two dimensions. Hundreds of times larger than the filament diameters, these values lie in the same range as the cyanobacteria *Geitlerinema* and *Pseudanabaena*, but are smaller than several strains of *Oscillatoria*. In contrast, the 2-Ga microfossil trichome *Halythrix*, is found to have a short correlation length of 29 ± 4 μm in two dimensions. Micron-wide pyritic replacement filaments observed in 3.23-Ga volcanogenic deposits also display a modest correlation length of 100 ± 15 μm in two dimensions. Sequences of species in two genera of our modern cyanobacteria possess tangent correlation lengths that rise as a power of the filament diameter D—$D^{3.3 \pm 1}$ for *Oscillatoria* and $D^{5.1 \pm 1}$ for *Geitlerinema*. These results can be compared with power-law scaling of D^3 for hollow tubes and D^4 for solid cylinders that is expected from continuum mechanics. Extrapolating the observed scaling behavior to smaller filament diameters, the measured correlation length of the pyrite filaments is consistent with modern *Geitlerinema* whereas that of *Halythrix* lies not far from modern *Oscillatoria*, suggesting that there may be structural similarities among these genera.

David Boal and Ray Ng. Department of Physics, Simon Fraser University, Burnaby, British Columbia V5A 1S6, Canada. E-mail: boal@sfu.ca

Accepted: 13 April 2010

Filament-forming cells have been present throughout much of the earth's history and first appeared more than three billion years ago, underlining their importance as a robust and efficient cell design (Barghoorn and Schopf 1966; Walsh and Lowe 1985; Schopf and Packer 1987; Schopf 1993; Rasmussen 2000; Furnes et al. 2004; see also Brasier et al. 2002). Among the morphologies of modern cyanobacteria that are thought to be the descendants of early cell lines, there are many examples of trichomes, with and without sheaths, having diameters and other shape characteristics similar to those of early cells. Three examples of 2-billion-year-old filamentous structures are displayed in Figure 1: parts A and B are *Gunflintia minuta* Barghoorn and *Gunflintia grandis* Barghoorn, respectively (Barghoorn and Tyler 1965; specimens from Lake Superior, Canada) and part C is *Halythrix* Schopf (Schopf 1968; specimen from Belcher Islands, Canada). The specimens are shown at low magnification to emphasize their sinuous appearance on a length scale of hundreds of microns; the apparent rigidity clearly varies from taxon to taxon. An example of the cyanobacterium *Geitlerinema* is shown later in the text at the same scale to demonstrate that modern filamentous cells may possess similar mechanical rigidity. Can the similarities and differences in shape between ancient and modern cells be described quantitatively, and can benchmarks be developed that would identify some structural aspects of microfossils that have been lost in the fossilization process itself?

The mechanical properties of modern cells can be studied in the lab with a variety of techniques involving active deformations, such as recording strain in response to stress, both to characterize the cell and to understand the functioning of its structural components. Even in static ensembles, the measured orientation, projected shape, and perhaps cross-sectional shape of modern cells provide data to quantitatively probe cell construction

 0094-8373/10/3604–0555/$1.00

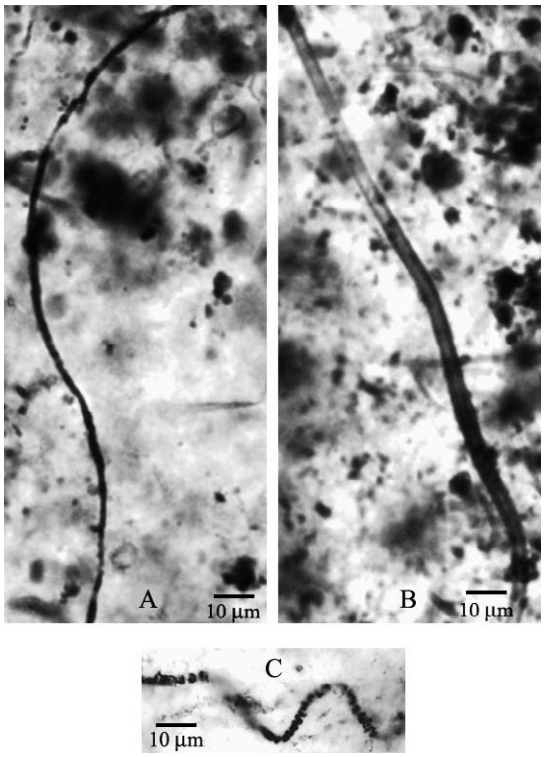

FIGURE 1. Examples of *Gunflintia minuta* (A) and *Gunflintia grandis* (B) from GSC 10913c (Schreiber, Ontario, Canada; author's material); *Halythrix* (C) from GSC 42769 (Belcher Islands, Canada; reported in Hofmann 1976). Scale bar, 10 μm in all images.

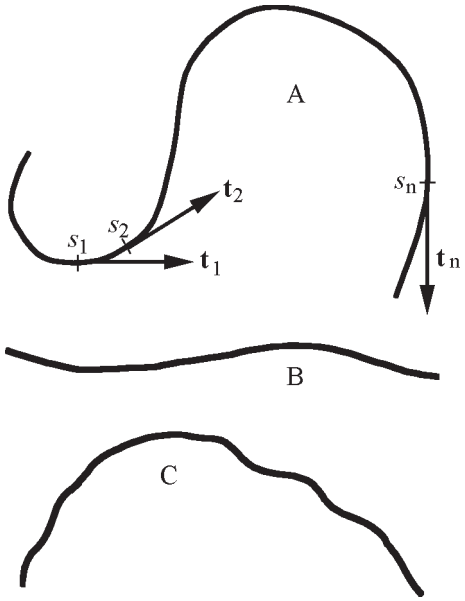

FIGURE 2. A, Unit tangent vectors ($\mathbf{t}_1$, $\mathbf{t}_2$, $\mathbf{t}_n$) at arc lengths (s_1, s_2, s_n) along a sinuous curve. Separations between the locations $\Delta s = |s_2 - s_1|$ are distances, not displacements. B, C, Typical shapes for curves, one with a tangent correlation length nine times its contour length (B) and another with a tangent correlation length equal to its contour length (C).

and some aspects of the division cycle. To the extent that the fossilization process preserves cell shape, or preserves the curvature of filaments, the same quantitative approaches based on shape analysis are relevant to microfossils as well as living cells. To briefly introduce one such analysis technique based upon static images of filaments, Figure 2A shows a sinuous curve along which a few tangent vectors **t** are drawn; the vectors have unit length (i.e., the dot product of the tangent vector with itself is unity: $\mathbf{t}_i \cdot \mathbf{t}_i = 1$). Arbitrarily choosing vector $\mathbf{t}_1$, we see that a nearby tangent vector $\mathbf{t}_2$ has a direction close to $\mathbf{t}_1$, whereas a distant vector $\mathbf{t}_n$ is generally not parallel to $\mathbf{t}_1$ at all. Thus, the ensemble average $<\mathbf{t}_i \cdot \mathbf{t}_j>_{\Delta s}$ (averaged over all pairs $\mathbf{t}_i$ and $\mathbf{t}_j$ separated by a fixed arc length Δs along the curve) should approach 1 at small Δs, where $\mathbf{t}_i$ and $\mathbf{t}_j$ are nearly parallel, and approach 0 at large Δs, where the tangent orientations are random. For a variety of very general situations, it can be established that $<\mathbf{t}_i \cdot \mathbf{t}_j>_{\Delta s}$ is described by the exponential function $\exp(-\Delta s/\xi_t)$, where ξ_t is *correlation length* and where the small and large Δs limits of $<\mathbf{t}_i \cdot \mathbf{t}_j>_{\Delta s}$ are 1 and 0, as required. The correlation length quantitatively captures how sinuous the curve is.

To gain some intuition about how the correlation length is related to the visual appearance of a filament, parts B and C of Figure 2 show two arbitrary curves with very different local curvature. The tangent correlation length of the relatively straight curve in panel B is about nine times its contour length, while that of the sinuous curve in panel C is equal to its contour length. To use physical systems as examples, ξ_t of *Gunflintia minuta* in Figure 1A is more than three times the contour length displayed in the image, whereas ξ_t of *Halythrix* in Figure 1C is one-third the contour length displayed. Another way to think about the correlation length is that ξ_t is the separation along the curve such that two unit tangent vectors are sufficiently de-correlated that their dot product is $1/e = 0.368$

on average, corresponding to an angle of 68 degrees. For a given contour length, the mean end-to-end displacement of a sinuous curve rises like the square root of the correlation length (see equation A2).

Here, using only static images, we determine tangent correlation lengths ξ_t for a suite of filamentous microfossils and what may be their modern cyanobacterial counterparts. At the very least, these correlation lengths provide a quantitative means of characterizing filamentous microfossils for comparison with each other and with modern cells. However, it also may be possible to glean insight into the structure of the specimen from its shape fluctuations and ξ_t, in spite of the fact that its cellular substructure is invisible. As a simple illustration, consider a biofilament whose relaxed configuration is straight, with very few direction-changing permanent defects in its construction. In a fluid medium with very mild random motion, such a filament will be sinuous with a tangent correlation length that depends on its mechanical stiffness: the stiffer the filament, the longer is ξ_t. Thus, if several genera of filamentous cells are present in a sample under the same fluid conditions, their relative stiffness can be obtained by comparing their correlation lengths.

The link between the stiffness of a filament and its mechanical components is provided by continuum mechanics. The resistance of a filament against bending is called its flexural rigidity, κ_f, which is related to the cross-sectional shape of the filament and to its elastic properties. For example, according to the classical theory of elasticity, κ_f of a uniform solid cylinder of radius R is proportional to the product of its Young's modulus and the fourth power of R, whereas that of hollow tubes is proportional to R^3 (see Appendix for details). In principle, the bending stiffness of structurally complex filaments can be obtained from knowledge of their construction and composition, although the resulting expression for κ_f may not have a simple, closed form. By measuring modern filaments, one can identify the most important contributions to κ_f from a variety of possible mechanical components. For example, the relative stiffness of a family of filaments with similar construction can be checked against the R^4 or R^3 scaling of solid or hollow tubes, revealing which components of a filament carry the greatest resistance to bending. Alternatively, by examining filaments with the same radius but chosen from different genera, one may be able to isolate the contribution of a mechanical component present in one genus but not in another.

The systematic study of modern filamentous cells provides a knowledge base that will be useful in determining the (hidden) structure of filamentous microfossils, or will aid in identifying common structural features among different taxa. For example, the sheath of some modern filaments has a higher Young's modulus than average for biomaterials, such that the presence of a sufficiently thick sheath will contribute significantly to κ_f because of the R^3 weighting it receives. In contrast, structural differences among filaments near their symmetry axis may be more difficult to detect, again owing to the R^n weighting.

In addition to the tangent correlation function, correlations in filament shape or cell length may provide additional tools for characterizing and revealing the structures of microfossils and their division cycle. For example, by imaging a filament (at a succession of focal regions) with its symmetry axis pointing toward the viewer, one can obtain the cross-sectional area of the filament as a function of location, $A(s)$, just as we obtain the behavior of the tangent vector $\mathbf{t}(s)$; consequently, a correlation length in area ξ_A can be extracted from the ensemble average of the product of the areas $<A_i\ A_j>$. The torsional deformation of a filament is also related to its shape and elastic properties, but the relevant elastic parameter is the material's shear modulus rather than its Young's modulus. This opens another possible route for probing the mechanical structure of filaments, although the measurement of torsion resistance even among modern filaments has not proven to be easy. Developing and applying the formalism for analyzing area and other shape correlations will be left to a separate publication.

An important aspect of this paper is the comparison of correlation lengths from both modern cyanobacteria and filamentous microfossils, concentrating on taxa with ages of about 2 Ga (Barghoorn and Tyler 1965; Cloud 1965; Hofmann 1975; Hofmann 1976; Awramik and Barghoorn 1977; Knoll et al. 1978). We report data for four microfossil taxa in this age range: *Gunflintia minuta*, *Gunflintia grandis*, *Eomycetopsis filiformis* and *Halythrix*, all having diameters around 1–4 μm. We used an additional unclassified filament with the same age to test the theoretically expected relation between the true correlation length of a filament in three dimensions and that determined from its two-dimensional projection. We also studied 3.23-Ga pyritic replacement filaments (Rasmussen 2000), which have smaller diameters of 0.5–2 μm. The suite of modern filamentous cyanobacteria used for comparison includes three species of *Oscillatoria* (PCC 6412, PCC 7112, PCC 8973), two *Geitlerinema* (PCC 7407, PCC 7411), and one *Pseudanabaena* (PCC 7403). As will be displayed later, these genera sample a range of conventional cell shapes that should include the microfossil taxa.

To briefly summarize the organization of this paper, we draw from three different disciplines to analyze a shared problem. Primarily working with new field samples, we assemble a collection of images of four filamentous microfossil taxa with enough filaments per taxon to obtain accurate values of the tangent correlation length ξ_t. A reference group of six cyanobacteria from the Pasteur Culture Collection is cultured and imaged, then analyzed within the same theoretical framework. This permits a comparative study of the tangent correlation lengths from both ancient and modern cells, as well as ξ_t that we extract from published images of 3.23-Ga pyritic filaments. Lastly, a few mathematical results for correlation lengths are developed and placed throughout the text as needed; a more detailed discussion of such results can be found in the Appendix.

Material and Methods

For now, we use the word filament generically without reference to the existence or structure of sheaths that may surround a trichome; such distinctions are introduced in later sections of the paper where the shape analysis is performed. Our sources of microfossil filament images come from published results, from new surveys of thin sections in established type collections, and from new microfossil-bearing material collected from two documented sites. In all cases, the overall shapes of the filaments do not appear to have undergone unidirectional strain since the time of deposition. By far the largest component of our analysis is based on 1.9-Ga fossil-laden chert gathered by one of the authors from the Gunflint Formation near Lake Superior, Canada (Barghoorn and Tyler 1965; Cloud 1965; age from Fralick et al. 2002). The localities investigated are the same as those of Barghoorn and Tyler (1965), namely a road cut 1.2 km northwest of Kakabeka Falls, Ontario, and the Lake Superior shoreline 6.4 km west of Schreiber, Ontario. The most promising collection sites were identified in surveys undertaken decades ago, such that only a few kilograms of fossil-bearing chert were needed to generate the results reported here. The region around Schreiber and neighboring Rossport contains isolated erosion remnants of the Gunflint Formation, whose primary surface exposure runs west about 160 km from Loon Lake to Gunflint Lake, Ontario. Barghoorn and Tyler (1965) and Cloud (1965), and references cited therein, describe the geology of this formation in detail, and identify its microfossil-bearing black chert as algal domes, which range up to 1.5 m in diameter at the Schreiber locality. As seen in thin section, the general appearance of the algal chert reported here is identical to that in Figure 2 of Barghoorn and Tyler (1965). Images for *Gunflintia minuta* and *Gunflintia grandis* were taken from three slides now deposited with the Geological Survey of Canada: GSC 10913a, GSC 10913c, and GSC 10914c.

Our second source of filaments is a collection of 2-Ga specimens from the Belcher Islands of Hudson Bay (Hofmann 1976), also part of the Geological Survey of Canada collection. Digital images are obtained for two taxa:

Eomycetopsis filiformis: 9 locations on GSC 43586,
Halythrix GSC 42769 (33.2*x*, 10.3*y*),

as well as one unclassified filament used for testing the properties of correlation functions:

Filament U GSC 43592 (27.0*x*, 16.0*y*).

The five-digit number is the GSC identification of the microscope slide, and the x,y coordinates are displacements in millimeters from its upper right-hand corner, with the slide label on the right, facing the objective lens. The *Halythrix* specimen is the same as that displayed in Plate 1, Figure 18 of Hofmann (1976). The samples are drawn mainly from the McLeary and Kasegalik Formations at several different stratigraphic levels; the McLeary formation itself is about 600 m thick. Found in black chert in stromatolitic dolostones, the sedimentary structure indicates deposition in supratidal, intertidal, and subtidal environments. The depositional environment and its relationship to modern algal mats are described by Hofmann (1975) and Golubic and Hofmann (1976).

Images of the oldest structures in our analysis are taken from Rasmussen (2000), who reports 3.23-Ga pyritic replacement filaments contained in volcanogenic massive sulphide deposits from the Pilbara Craton in Western Australia (age from Buick et al. 2002). The deposit itself is thought to have originated in a deep-sea marine environment at water depths probably exceeding 1000 m (see Vearncombe et al. 1995 for further details on the depositional environment). The diameters of the filaments are 0.5–2 μm, with samples analyzed here being close to 1 μm. Our analysis is based on the locus of the central contour of the track, which we obtain from digital images accompanying the original publication; the variation in the track width is not important to our analysis in this particular case. Six filaments selected from Figure 3 of Rasmussen (2000) have rather short contour lengths compared to the Gunflint taxa and our modern cyanobacteria, although they are long enough to yield a tangent correlation length.

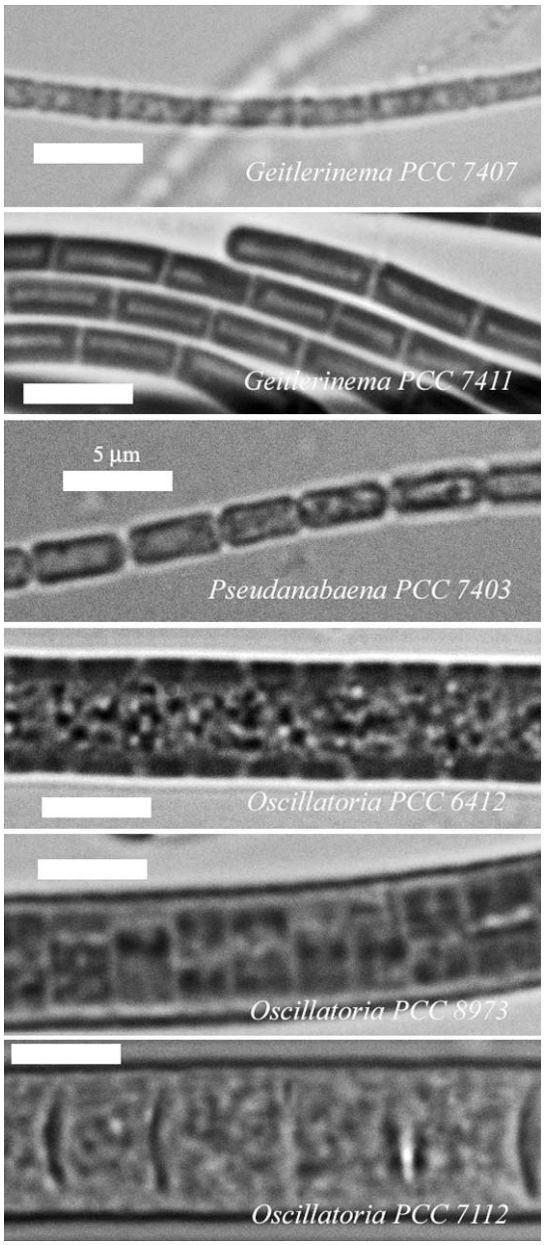

FIGURE 3. Examples of six filamentous cyanobacteria cultured for this study. Scale bar, 5 μm in all images.

The modern cyanobacteria reported in this study are six strains of *Oscillatoria* (PCC 6412, PCC 7112, PCC 8973), *Geitlerinema* (PCC 7407, PCC 7411), and *Pseudanabaena* (PCC 7403); examples of each strain are displayed in Figure 3 to illustrate the range of filament diameters. Two additional strains of *Pseudanabaena* (PCC 6901, PCC 6903) were also successfully cultured and imaged. However,

the mean length of the filaments in the cultured populations proved to be too short to provide an accurate correlation length, so data from these two species of *Pseudanabaena* are not displayed. The strains were obtained from the Pasteur Culture Collection (Paris, France) and cultured in the appropriate medium (BG11 for all strains except PCC 7403 for which $BG11_0 + 2$ mM $NaNO_3$ is used; both solid and liquid media were supplemented with $NaHCO_3$ to 10 mM); for solid media, agar was used at 0.6% (for further details of media preparation, see Atlas 2004: p. 210 and Rippka 1988). Samples were cultured in an incubator (Thermoelectron Corp. model 818) at 20°C with 12 hour light/dark cycles. To image the filaments, a drop of a cell suspension created by very mild agitation (approximately 10^6 cells/mL) was placed on a glass microscope slide that was then overlain with a glass coverslip, trapping the suspension as a thin layer. In most cases, the ensemble of images for a given taxon consisted of ten or more filaments selected according to both their length and the restriction that a given filament did not have lateral contact with a neighbor; mean filament lengths in the images varied from 400 to 700 μm. The exceptional case was *Pseudanabaena* PCC 7403, from whose population of generally short filaments (40 μm in our cultures) 30 specimens had to be taken to generate a correlation length with acceptable accuracy.

Depending on the mode of analysis, images of the filaments are captured using Olympus BX51 or IX51 optical microscopes outfitted with CoolSNAP© *cf* CCD cameras from Roper Scientific (pixels of 4.65 μm to the side). Among modern cyanobacteria, *Geitlerinema* are imaged at 10×, *Oscillatoria* at 20×, and *Pseudanabaena* at 40×. In general, correlation lengths are best extracted from long filaments, which favors the selection of specimens with their symmetry axis perpendicular to the viewer, permitting them to be seen lengthwise. Determination of the filament contour is done manually: the grayscale image profile transverse to the filament axis is searched at 10–20 pixel intervals (along the axis) to find its midpoint, a procedure that is usually accurate to better than a single pixel compared to contour lengths of 500–1200 pixels for microfossils, and much longer for most of the modern cyanobacteria. The tangent to the contour is obtained numerically from the locus of these midpoints by constructing the unit vector between pairs of points separated by one intermediate point (that is, a unit tangent vector is constructed from next-nearest-neighbor points, and its orientation is assigned to the physical location of the intermediate point). We perform a three-dimensional reconstruction of a particular microfossil *Filament U*, where the x,y,z coordinates of the contour can be taken accurately; for all other microfossil taxa, the analysis is performed on two-dimensional projections of the specimen. Our modern cyanobacteria are prepared as two-dimensional specimens, so that images of their loci are not projections of a three-dimensional shape.

Tangent Correlation Function

Changes in the local orientation of the sinuous curve illustrated in Figure 2A can be recorded through the behavior of the tangent vector $\mathbf{t}(s)$ at location s along the curve, where $\mathbf{t}$ has unit length according to the dot product $\mathbf{t}\cdot\mathbf{t} = 1$. If two location s_1 and s_2 are close to each other on the curve, then $\mathbf{t}(s_1)$ and $\mathbf{t}(s_2)$ have similar directions and their dot product is close to unity. On the other hand, if s_1 and s_2 are far apart along the curve (even though they may be close spatially), their tangent vectors may point in quite different directions and $\mathbf{t}(s_1)\cdot\mathbf{t}(s_2)$ may vary between −1 and +1. The words ''far apart'' imply that there is a distance scale associated with the fluctuations in orientation, a distance that can be extracted from the tangent correlation function $C_t(\Delta s)$,

$$C_t(\Delta s) \equiv \langle \mathbf{t}(s_1)\cdot\mathbf{t}(s_2)\rangle. \quad (1)$$

The ensemble average indicated by the brackets $< \ldots >$ on the right-hand side of this equation is performed over all pairs of points s_1 and s_2 subject to the constraint that $|s_2 - s_1|$ is equal to a particular Δs specified on the left-hand side; i.e., Δs is the distance

between the points as measured along the curve. When s_1 and s_2 are nearby ($\Delta s \cong 0$), the ensemble average over $\mathbf{t}(s_1)\cdot\mathbf{t}(s_2)$ is necessarily close to unity, whereas when Δs is so large such that the tangent orientations are random with respect to each other, the average is close to zero. This behavior of $C_t(\Delta s)$ at small and large Δs might be described by either power law decay in Δs or by exponential decay, and it turns out that for a variety of very general situations, exponential decay is the correct description (see Boal 2002 and references therein):

$$C_t(\Delta s) = \exp(-\Delta s/\xi_t). \quad (2)$$

The length scale for the correlations is provided by the tangent correlation length ξ_t: the more sinuous the curve, the smaller is ξ_t. Figure 2 displays two examples of the visual appearance of sinuous curves as a function of the ratio of the tangent correlation length to the contour length.

The accuracy to which ξ_t can be determined depends, of course, on the number of points used in constructing $C_t(\Delta s)$. Suppose that a curve is sampled at n points along its contour length (the total length of the filament as measured along its contour), each separated from its neighbors by identical distances S along the curve, as illustrated in panel A of Figure 2. Then there are $n - 1$ pairs s_1 and s_2 separated by S, the smallest difference available in the data set, but far fewer pairs at separations large compared to S. Given the finite length of a filament in an experimental situation, the largest Δs for which a given curve can provide an accurate C_t is much less than the overall length of the filament. Hence, it may be difficult to evaluate C_t at separations Δs that are even a few times the applicable correlation length ξ_t. To measure C_t more accurately, we collect data from many filaments in the same environmental setting: typically 5–10 microfossil filaments of a given taxon and 10 filaments of a modern cyanobacterium. The two notable exceptions are the microfossil *Halythrix*, for which we identified only one example long enough for analysis, and the modern *Pseudanabaena* PCC 7403, whose filaments are sufficiently fragile that the measured ensemble consisted of 30 short sections. Thus, our methodology is closer to the situation displayed in panel B of Figure 4, where tangent pairs at the same Δs are taken from many filaments to construct the ensemble average.

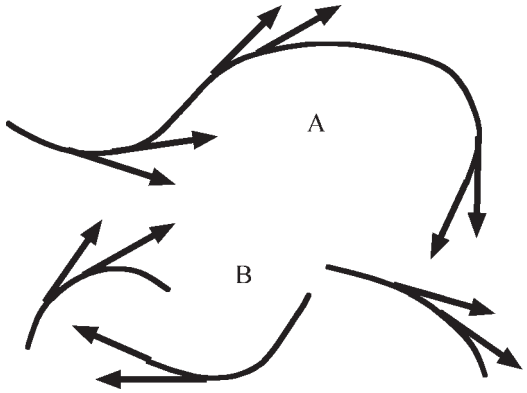

FIGURE 4. Two approaches to constructing tangent correlation functions. A, Many tangent pairs are obtained from a long filament. B, The pairs are taken from a large number of short filaments in the same physical ensemble.

The last aspect of C_t deserving discussion is the dimensionality of the system under investigation. No reference is made in equation (1) to whether the curve travels through three-dimensional space, or through two dimensions, or is a projection of a three-dimensional trajectory onto a two-dimensional plane; the exponential decay applies in all cases, but not necessarily with the same correlation length. For the living cyanobacteria studied here, the sample is confined between a microscope slide and a glass cover slip, forcing it to lie in a two-dimensional plane; in this case, we denote the correlation length by ξ_2 to reflect its two-dimensional origin. For most of the microfossils, the observed filament, by necessity, lies within a slice about 50 μm thick and is generally imaged with a low-magnification objective lens so that the entire filament is in focus simultaneously. In this case, the correlation length is obtained from a two-dimensional projection of a three-dimensional trajectory, and is denoted by ξ_{2p}. Finally, the microfossil *Filament U* is sufficiently sinuous that we have been able to reconstruct the path of one specimen in three dimensions by stepping the focal plane through the 50-μm thin section by means of a 50 objective with a narrow

depth of field. For this filament, we are able to obtain both ξ_3 from the three-dimensional shape as well as ξ_{2p} from its projection. In the Appendix to this paper, we show that these two correlation lengths should obey

$$\xi_3 = (3\pi/8)\xi_{2p}, \qquad (3)$$

a relationship that can be tested by our measurements. Given that the numerical factor $3\pi/8$ is only equal to 1.18, the difference between the various methods of obtaining the correlation length is not large. Nevertheless, it should be kept in mind that different methods of obtaining C_t may lead to different values for ξ_t.

Microfossil Correlation Lengths

Inferring the original structure of microfossil filaments from their preserved form is not without ambiguity. *E. filiformis* are relatively uniform hollow tubes (Hofmann 1976), as are the *G. grandis* specimens of our ensembles, illustrated in Figure 1B. However, *G. grandis* may also have the appearance of a sheathless trichome with irregularly shaped cells separated by visible cross walls (Barghoorn and Tyler 1965), although such trichomes are not included among the objects analyzed here. Some *G. minuta* also have a tube-like appearance, whereas others in our ensemble are visually opaque or resemble the laterally shrunken remains of the original filament. Thus, the cell widths extracted from filamentous microfossils may be less than the native widths. Lastly, *Halythrix* is described as a flexible trichome, as displayed in Figure 1C. Although these microfossils will be referred to collectively as filaments, their specific structure will be highlighted when it is relevant.

In choosing individual filaments for imaging purposes, care is taken to avoid regions where the filaments are oriented because of their location within a planar mat, or by their stretch around obstacles, or entanglement around neighbors or by their alignment induced by flow. In other words, we choose filaments from regions of low cell density where the influence of environment on filament shape is reduced. Among the microfossil taxa studied here, the most statistically

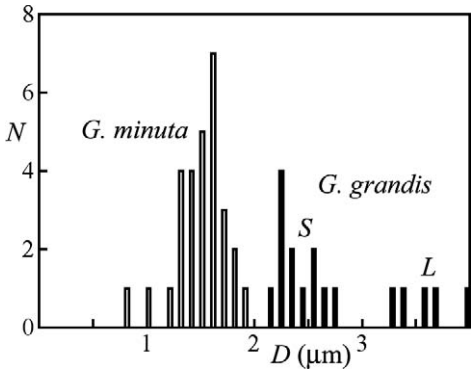

FIGURE 5. Size distributions as a function of mean diameter D (in μm) of 1.9-Ga *Gunflintia minuta* (hollow bars, 29 filaments) and two subsets of *Gunflintia grandis* (solid bars): set *S* has diameters of 2–3 μm (12 filaments) and set *L* has diameters of 3–4 μm (5 filaments). The number of filaments per 0.1 μm interval is N. Specimens are taken from GSC 10913a, GSC 10913c, and GSC 10914c.

accurate determination of tangent correlation lengths is obtained from Gunflint chert, prepared in 50-μm-thick sections to capture a greater fraction of an undulating filament. From surveys of three such sections, 46 of the longest examples of *Gunflintia* were imaged for analysis. Figure 5 displays the distribution of filament diameters of this population in intervals of 0.1 μm, recognizing that the diameter of an individual filament may vary by up to ±0.2 μm along its symmetry axis. Although the number of counts per interval is not large, we choose to segregate the filaments into three groups for the purpose of discussion. Adopting the classification scheme of Barghoorn and Tyler (1965), we assigned 29 filaments with diameters of 1–2 μm to *G. minuta*, and 17 to *G. grandis* (2–4 μm), which we further divided into two subsets of 12 small (*S*, 2–3 μm diameter) and 5 large (*L*, 3–4 μm diameter) filaments. Barghoorn and Tyler (1965) emphasize that such a broad distribution of diameters may indicate the presence of more than one or two taxa. The typical contour lengths in the Gunflint samples are 180 μm for *G. minuta*, 140 μm for *G. grandis S*, and 180 μm for *G. grandis L*.

Contributions to the tangent correlation function $C_t(\Delta s)$ for each range of $\Delta s = |s_2 - s_1|$ are collected from each filament in order to construct a weighted average over the whole filament set or subset. If one chose to average

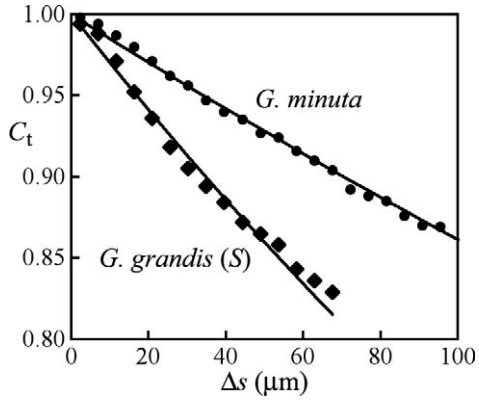

FIGURE 6. Tangent correlation function $C_t(\Delta s)$ as a function of separation Δs (in μm) obtained by weighted average for *G. minuta* (disks) and the *S* group of *G. grandis* (diamonds), whose ensemble size is given in Figure 5. The solid curves are the exponential decays predicted by equation (2), with $\xi_{2p} = 670$ μm and 330 μm for *G. minuta* and the *S* group of *G. grandis*, respectively.

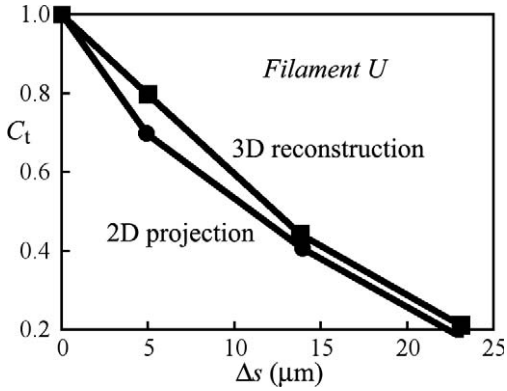

FIGURE 7. Tangent correlation function $C_t(\Delta s)$ as a function of separation Δs (in μm) for a single specimen of 2-Ga *Filament U* as obtained from a three-dimensional reconstruction (squares) and from its two-dimensional projection (disks). The extracted correlation lengths are $\xi_{2p} = 14.7 \pm 1.0$ μm in two dimensions and $\xi_3 = 18.4 \pm 2$ μm in three dimensions. Specimen is from GSC 43592 (collected by H. Hofmann, Belcher Islands, Canada).

over all available Δs in all filaments, then the longest filaments would unduly influence the behavior of $C_t(\Delta s)$ in the regime where Δs exceeded the contour lengths of the shorter filaments in the population. Hence, $C_t(\Delta s)$ is quoted to a maximum value of Δs that is appropriately *smaller* than the length of the shortest filament in the ensemble. When averaged over our filament ensembles, the product $\mathbf{t}(s_1)\bullet\mathbf{t}(s_2)$ contains 200–4000 contributions at each interval in Δs, depending on the taxon. The resulting correlation functions are shown in Figure 6 for projected filament trajectories in two dimensions, leading to the determination of the correlation length ξ_{2p}. The figure shows the raw data as well as their fit with an exponential function. *G. minuta*, the narrower of the two taxa, is found to have $\xi_{2p} = 670 \pm 40$ μm. In contrast, the wider *G. grandis* has a shorter ξ_{2p} of 330 ± 30 μm and 390 ± 40 μm for the *S* and *L* subsets, respectively. The fact that ξ_{2p} of the *S* and *L* populations agree to within statistical uncertainties may support their assignment as one taxon; however, ξ_{2p} should differ by more than a modest 20% between the *S* and *L* subgroups, judging from the behavior of the stiffness of the filaments expected from their diameters, as described below.

Of the two taxa studied from the Belcher Islands microfossils, *E. filiformis* is visually similar to *G. minuta*, which has a mean diameter of just ~1.5 μm; in the samples measured here, *E. filiformis* filaments possess a slightly larger mean diameter of 2.2 μm (standard deviation = 0.2 μm) and contour lengths that average about 120 μm. Nine filaments were imaged to generate an ensemble-averaged C_t, following the same method described above for *Gunflintia*. Owing to the much smaller set of filaments, the quality of the data is not as good as that shown in Figure 6 for *G. minuta*, such that the extracted correlation length $\xi_{2p} = 700 \pm 100$ μm has a much larger estimated error. As with the *Gunflintia* specimens, the curvature of the filaments in three dimensions is so gentle that undulations in the *z* direction are difficult to record accurately; as a result we are unable to apply equation (3) as a test.

Filament U in the collection of 2-Ga microfossils from the Belcher Islands of Hudson's Bay (Hofmann 1976) provides a good laboratory for exploring the validity of applying the correlation length concept to filamentous microfossils; it has a contour length of a healthy 160 μm and is mostly contained within its thin section (GSC 43592). Images of the filament were taken in 1-μm steps in the vertical (observational) direction, permitting the three-dimensional shape to be approximately reconstructed. Figure 7 displays the tangent correlation function obtained from

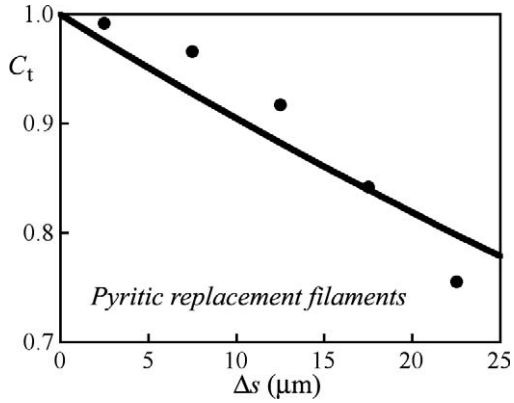

FIGURE 8. Tangent correlation function $C_t(\Delta s)$ as a function of separation Δs (in μm) for pyritic replacement filaments from 3.23-Ga volcanogenic deposits as reported by Rasmussen (2000). The solid curve is a fit to the data (solid circles) using an exponential function with $\xi_{2p} = 100$ μm.

the two-dimensional projection of this filament and from the three-dimensional reconstruction; that is, ξ_{2p} is extracted from unit vectors tangent to the projected image, whereas ξ_3 is obtained from vectors tangent to the reconstructed contour. The tangent correlation functions $C_t(\Delta s)$ from the two approaches are not dissimilar: $\xi_{2p} = 14.7 \pm 1.0$ μm and $\xi_3 = 18.4 \pm 2$ μm from the initial decay of C_t up to $\Delta s = 20$ μm; these are firm results in the sense that the contour length is eight to ten times longer than the relevant ξ. From equation (3), the three-dimensional correlation length ξ_3 should be $3\pi/8 = 1.18$ times its two-dimensional cousin ξ_{2p}, a prediction that is within the uncertainty of the ratio 1.25 ± 0.1 observed here. The measured ratio lends additional but cautious support to the use of tangent correlation lengths as valid characterizations of filamentous microfossils in two and three dimensions. Our *Halythrix* specimen (GSC 42769) has a shorter contour length (70 μm) and yields ξ_{2p} of 29 ± 4 μm, where the error does not quantitatively recognize the small contour length of the specimen. In any event, the measured correlation length of *Halythrix* is *much* shorter than those of the *Gunflintia* and *E. filiformis* taxa described above, whose values of ξ_t are hundreds of times their diameter, whereas ξ_t of *Halythrix* is just an order of magnitude larger than its diameter. As will be shown below, this difference may be related to the underlying architecture of the filaments.

TABLE 1. Measured diameters and tangent correlation lengths for four taxa of 2-Ga filamentous microfossils as well as 3.23-Ga pyritic replacement filaments, with the source of the samples as indicated. *Halythrix*, *E. filiformis*, and *Filament U* are drawn from material reported by Hofmann (1976); *Gunflintia* specimens are new material reported here. Samples with GSC labels are part of the Geological Survey of Canada collection.

Source	Diameter (μm)	ξ_{2p} (μm)	ξ_3 (μm)
Halythrix GSC 42769	2.3 ± 0.2	29 ± 4	
E. filiformis GSC 43586	2.2 ± 0.2	700 ± 100	
G. minuta GSC 10913a,c 10914c	1–2	670 ± 40	
G. grandis (*S*) GSC 10913a,c 10914c	2–3	330 ± 30	
G. grandis (*L*) GSC 10913a,c 10914c	3–4	390 ± 40	
3.23-Ga pyritic filaments Rasmussen (2000)	~1	100 ± 15	
Filament U GSC 43592	2.3 ± 0.2	14.7 ± 1.0	18.4 ± 2

Finally, we come to the collection of 3.23-Ga pyritic replacement filaments obtained by Rasmussen (2000). As they appear in thin section, the contour lengths of the objects may exceed 100 μm, although the samples we imaged are 25–65 μm long; the track diameters lie around 0.5–2 μm, similar to *G. minuta*. We constructed the usual tangent correlation function $C_t(\Delta s)$ from published images of six of the longer tracks; each interval in Δs of 10 μm received 25–100 contributions to each $\langle \mathbf{t} \cdot \mathbf{t} \rangle$. The resulting tangent correlation function C_t is shown in Figure 8, along with the exponential decay of equation (2) with $\xi_{2p} = 100 \pm 15$ μm, where the uncertainty is estimated from the number of counts per Δs interval. The true uncertainty may be larger than 15 μm because the contour lengths of the filaments in this particular group are fairly short. All of the results from our analysis of filamentous objects in the 2–3-μGa age range are summarized in Table 1 and will be displayed graphically below, where they are compared with the properties of modern filamentous cyanobacteria.

For completeness, mention should be made of the non-biological origin of some filamentous forms observed in chert, namely carbonate- or quartz-filled trails that can form

behind minute (1–10 μm) pyrite grains migrating in the chert matrix (Tyler and Barghoorn 1963; Knoll and Barghoorn 1974). Examples of such trails do occur in our Gunflint specimens, but with a much smaller ratio of contour length to filament diameter than what is characteristic of the filaments we have selected for analysis. Pyrite appendages, which may have contour lengths of 100 μm, commonly have a length-to-diameter ratio of ten or less, which is an order of magnitude smaller than our suite of filamentous objects.

Cyanobacterial Correlation Lengths

The number of modern filamentous cyanobacteria and (eukaryotic) green algae that can be cultured and characterized is clearly much larger than the suite of microfossil taxa studied here. From the Pasteur Culture Collection we selected six filamentous cyanobacteria having diameters that overlap with the microfossil taxa but span a large enough range to permit the testing of the width-dependence of ξ_t expected from continuum mechanics (two additional strains of *Pseudanabaena* that we cultured did not yield long enough filaments for analysis). Figure 3 displays short segments of these six strains, all drawn at the same scale to demonstrate the range of filament width—from narrow *Geitlerinema* to thick *Oscillatoria*. *Geitlerinema* does not have a permanent sheath, although some species of *Oscillatoria* may be surrounded by a mucilagenous tube within which the filamentous assembly of cells may glide, depending on how the sample is grown; this arrangement is observed for our culture of *Oscillatoria* PCC 8973, for example. *Pseudanabaena* may also exhibit a diffuse mucilagenous envelope. Our cyanobacteria are freshwater species and are motile, with the exception of *Pseudanabaena* PCC 7403.

The filaments in almost all of our cultured strains are long, such that only ten filaments are needed to construct C_t with reasonable accuracy for a given strain. The exception is *Pseudanabaena* PCC 7403: its filaments are fragile and consequently short, even though the mixing process in sample preparation is very gentle. As a result, an ensemble of 30 filaments was needed for constructing C_t for PCC 7403, with contour lengths that were always less than the measured tangent correlation length. Just as with the microfossil samples, care was taken to select for analysis those filaments with shapes that were not obviously influenced by the growth environment. In our process for imaging cyanobacteria, the filaments are held flat between a microscope slide and a cover slip, such that the measured correlation length is ξ_2, not ξ_{2p} of the microfossil taxa. We have not attempted to prepare a deeper specimen chamber to hold a filament rigidly in three dimensions, which would permit equation (3) to be tested in the context of living cells.

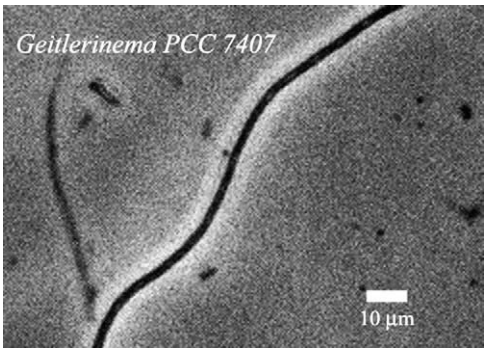

FIGURE 9. Image of the modern cyanobacterium *Geitlerinema* PCC 7407, taken with a 10× phase contrast (Ph 1) objective.

As a group, the genera that have been selected represent three very different cell geometries. The individual cells of *Geitlerinema* are approximately four times as long as they are wide, in contrast to *Oscillatoria*, where the mean cell lengths of our strains are only about 70% of their widths. Between these two situations is *Pseudanabaena* with a mean cell length about 1.5–2 times the cell width. Note that *Pseudanabaena* also has a more pronounced indentation at the cell division plane than the other two genera have. The narrowest of our cyanobacterial filaments are the two strains of *Geitlerinema*, one of which is shown in Figure 9 using an image from phase contrast optics. The figure is drawn to the same scale as Figure 1 to illustrate the qualitatively similar appearance to *Gunflintia minuta*, which has a slightly smaller diameter (although we recognize that the preserved diameter of the microfossil may not have been its native diameter).

TABLE 2. Measured diameters and tangent correlation lengths (ξ_2) for six strains of filamentous cyanobacteria obtained from the Pasteur Culture Collection.

Strain	Diameter (μm)	ξ_2 (μm)
Geitlerinema PCC 7407	1.5 ± 0.2	465 ± 50
Geitlerinema PCC 7411	2.1 ± 0.2	2600 ± 200
Pseudanabaena PCC 7403	2.1 ± 0.2	480 ± 50
Oscillatoria PCC 6412	5.5 ± 0.6	1300 ± 130
Oscillatoria PCC 8973	6.5 ± 0.7	1700 ± 170
Oscillatoria PCC 7112	7.7 ± 0.8	3900 ± 400

The tangent correlation lengths from our cyanobacterial ensembles are typically within a factor of two of a millimeter, ranging from a few hundred to a thousand times the filament diameter, as summarized in Table 2 and Figure 10. Of the three genera displayed in Figure 10, both *Geitlerinema* and *Oscillatoria* exhibit values of ξ_2 that rise with filament diameter, which is expected on theoretical grounds if the members of a given genus have similar architecture and construction. There is an overall tendency for ξ_2 to grow with diameter across all strains, yet the structural differences between families obviously have a large effect on ξ_2: for example, the correlation length of 2-μm-wide *Geitlerinema* is notably larger than that of 5–6-μm-wide *Oscillatoria*. The statistical uncertainties in these results are comparable to the correlation functions of the microfossil taxa such as displayed in Figure 6. The motivation behind the straight lines in the figure will be explained in the following section.

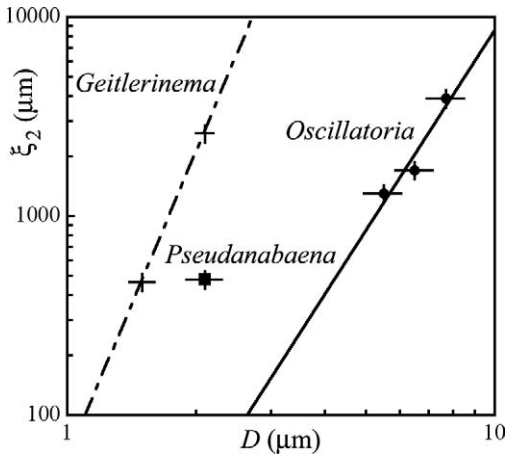

FIGURE 10. Measured ξ_2 (in μm) for filamentous cyanobacteria as a function of their mean diameter D. The correlation functions are approximately described by $4.3 \cdot D^{3.3 \pm 1}$ for *Oscillatoria* and $62 \cdot D^{5.1 \pm 1}$ for *Geitlerinema* (solid and dot-dashed lines, respectively; both D and the result are in μm). The cyanobacteria are *Geitlerinema* (crosses), *Pseudanabaena* (square), and *Oscillatoria* (disks).

Comparison of Ancient and Modern Cells

Several different effects can contribute to the sinuous appearance of a cellular filament. First, the cell growth and division processes may generate imperfections on distance scales of a few to tens of cell lengths that would introduce variation in the direction of growth. For example, if the cross wall or neck region between successive cells of a trichome is not exactly on its symmetry axis, there will be small changes in the local orientation of the trichome that, in some cases, could accumulate over tens of cell lengths to generate measurable curvature along the filament. However, curvature introduced at the linkage point between cells that arises from non-axial division is permanent in the sense that the polar angle between cells (but not necessarily the azimuthal angle) would be fixed at division. Among our modern cyanobacteria, we see no evidence for this effect, at least over distances along the contour of 20 or more cells: when subjected to shear flow and observed microscopically, the filaments change direction smoothly with no obviously permanent kinks (except in a few unusual instances). Similarly, we see no evidence for permanent domains of curvature arising from inhomogeneities or gradients of the growth medium. Hence, we discard off-axis cell division as the source of curvature measured here.

Curvature could also be introduced through the buckling of a motile filament if the force driving the motion is large enough. Buckling can arise when the leading end of the filament experiences resistance to its motion as it encounters other filaments or immobile objects. We see evidence for buckling among our motile cyanobacteria and, as a result, choose to analyze filaments from an environment with low cell density so as to avoid filaments that are in contact with one another. Although we use similar criteria for selecting microfossil specimens, we are not able to judge their effectiveness in avoiding

this source of curvature in the microfossil context.

A third means of generating curvature is through the response of the filament to random local shear fields and this is what we assume is the situation here. Now, the deformation of a filament in response to a shear stress is inversely proportional to the filament's stiffness or, properly speaking, its *flexural rigidity* κ_f: the stiffer the filament, the smaller the deformation for a given stress. As described further in the Appendix, the deformation energy per unit length for bending a uniform rod is proportional to $\kappa_f/2$ multiplied by the square of the rate of change of the tangent direction along the filament contour. This is just like Hooke's Law for springs, where the deformation energy for stretching is proportional to one-half of the spring constant multiplied by the squared length of the deformation.

The flexural rigidity depends on the cross-sectional shape of the filament and on the elastic properties of its components. Mathematical expressions for κ_f can be derived within the formalism of continuum mechanics, and the starting point for our presentation is the bending rigidity a uniform solid rod of circular cross-section. Beginning with equation (A6), one can show that the flexural rigidity of a solid cylinder of radius R is equal to $\pi Y R^4/4$, where Y is the Young's modulus of the material; typically $Y \sim (1\text{–}5) \times 10^8$ J/m^3 for soft biomaterials. It's easy to use this expression to determine κ_f of a hollow cylinder by simply subtracting the core from an initially solid cylinder: for a hollow cylinder of outer radius R bounded by a wall of thickness t, one finds κ_f is exactly $\pi Y[R^4 - (R\text{-}t)^4]/4$. This can be approximated by $\kappa_f \cong \pi Y R^3 t$ for a hollow tube with a thin wall relative to its radius (i.e., when $t \ll R$), as can be seen by expanding $(R\text{-}t)^4$ and keeping only the leading order term in t.

It should be clear how to construct κ_f for composite systems with varying Young's modulus by taking a sum over concentric cylinders. Thus, one can formally write $\kappa_f = (\pi/4)\ \Sigma_i\ Y_i\ (R_{i,\text{outer}}{}^4 - R_{i,\text{inner}}{}^4)$, where i is an index referring to each mechanical component of the system. The R^4 factor means that the outer structural components of the filament have the greatest influence on κ_f and the core has the least influence, all other things being equal. Thus far, no systematic studies of modern filamentous cells have been undertaken to identify the contributions of the various components to κ_f, although the elastic properties of the components in isolation have been measured for a selection of cells (reviewed in Boal 2002). Thus, we see that the flexural rigidity grows as R^3 or R^4 for the rod and tube geometries. Given that the energetic cost of the deformation is proportional to κ_f, it would not be surprising if the tangent correlation length were also proportional to R^3 or R^4, as a benchmark.

We now examine the data in Figure 10 within the context of continuum mechanics. First, there is no reason to believe that all filamentous cells will possess the same flexural rigidity: the radii, sheath thickness (if any), and Young's modulus all influence κ_f. However, given the expressions that we have just obtained, κ_f depends most strongly on the filament radius, as R^3 or R^4. Further, even for hollow tubes, t may increase with R as well, giving an effective dependence of κ_f on R as something higher than the third power. Thus, in the extreme situation that the construction and chemical composition of the structurally important components of the filaments were the same across all genera, then one might expect that a single function $\kappa_f = CR^n$ with a universal value of the proportionality constant C can describe all filaments. Of course, this is not the case and there are many structural differences among even the three genera in Figure 3, so the most likely behavior of κ_f is that species within a given genus obey a particular R^n scaling, but the proportionality constant C will vary from one genus to another. For a filament subject only to thermal fluctuations in its deformation energy, the correlation length ξ_t is linearly proportional to the flexural rigidity κ_f: the exact expression is $\xi_t = \kappa_f/k_BT$, where k_B is Boltzmann's constant and T is the temperature (see Boal 2002 for details). We assume that this proportionality is also valid here, so that the expected functional form of the correlation length remains $\xi_t = CR^n$, where the propor-

tionality constant C varies with the genus. Hence, a logarithmic plot of ξ_t versus R should be a straight line with a slope of 3 or 4 associated with the power law dependence of κ_f on R.

The tangent correlation lengths of three genera of cyanobacteria are plotted in Figure 10, but for one of these, *Pseudanabaena*, there is only one datum. As mentioned in ''Materials and Methods,'' two of the three species of *Pseudanabaena* that we cultured (PCC 6901 and PCC 6903) possessed such short filaments that we were unable to determine their correlation lengths; consequently, we cannot study the power-law scaling of ξ_t for this genus. However, there is a modest amount of data for *Geitlerinema* and *Oscillatoria*, which we attempt to represent by $\xi_2 = CD^n$, where D is the filament diameter. The two straight lines shown in Figure 10 are the functions $\xi_2 = 62 \cdot D^{5.1 \pm 1}$ for *Geitlerinema* and $\xi_2 = 4.3 \cdot D^{3.3 \pm 1}$ for *Oscillatoria*, where D must be quoted in microns, and the result for ξ_2 is also in microns. The exponents in these functional forms, 5.1 ± 1 and 3.3 ± 1, are seen to be in good agreement with the expectations from continuum mechanics for the D-dependence of the flexural rigidity. One characteristic that distinguishes among the three genera of Figure 10 is the mean length-to-width ratio of the individual cells: roughly 4 for *Geitlerinema*, 1.5–2 for *Pseudanabaena*, and 0.7 for *Oscillatoria*. Thus, we observe that for a fixed cell diameter, ξ_2 increases with the length-to-width ratio of the cell. Given the very large difference between the cell length-to-width ratios of *Geitlerinema* and *Oscillatoria*, we conjecture that these two genera lie near two distinct soft limits for the range of tangent correlation lengths available to cellular filaments. That is, with its large length-to-width ratio of individual cells, *Geitlerinema* represents one limit, and the small length-to-width ratio of *Oscillatoria* represents the opposite limit.

To interpret ξ_t from our microfossil measurements in the context of modern cyanobacteria, the microfossil data from Table 1 are plotted in Figure 11, although to a vertical scale that has been shifted by one order of magnitude relative to the cyanobacteria of Figure 10 such that the lower half of Figure 10 is the same domain of ξ_2 as the upper half of Figure 11. In addition, the functions describing ξ_2 of *Geitlerinema* and *Oscillatoria* are plotted in Figure 11, with the lower half of the figure representing an extrapolation by up to an order of magnitude. For clarity, data from modern filaments are not displayed on Figure 11: data from modern *Geitlerinema* and *Pseudanabaena* are in the same range as microfossil taxa *Gunflintia* and *E. filiformis*. This overlap unfortunately tends to confuse the figure even though the data help to interpret the results.

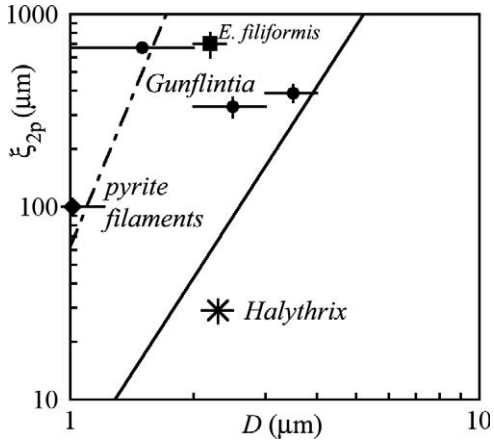

FIGURE 11. Measured ξ_{2p} (in μm) for microfossil filaments as a function of their mean diameter. The curves $4.3 \cdot D^{3.3 \pm 1}$ and $62 \cdot D^{5.1 \pm 1}$ (both D and the result are in μm) are drawn for reference and also appear in Figure 10. The filaments are *Gunflintia* (disks), *Halythrix* (cross), and *E. filiformis* (square); pyritic replacement filaments are indicated by the diamond near the y-axis.

The first observation in comparing Figures 10 and 11 is that the tangent correlation lengths of the microfossils are easily in the same range as modern filamentous cyanobacteria. However, this similarity by itself does not imply that our microfossil taxa must be cyanobacteria, because the correlation lengths of eukaryotic green algae with similar diameters also lie in this range; for example, $\xi_2 = 900 \pm 100$ nm for the green alga *Stichococcus* with a mean diameter of 3.5 ± 0.2 μm (Boal and C. E. Forde, unpublished). Let's examine the correlation lengths of each microfossil taxon in turn, beginning with *E. filiformis*. At 700 ± 100 μm, ξ_{2p} of *E. filiformis* is not far

from the functional fit to ξ_2 of *Geitlerinema* represented by the dot-dashed line on the figure. The two types of filaments also have a similar visual appearance as tubelike structures. In addition, *E. filiformis* is not that far removed from $\xi_2 = 480 \pm 50$ of modern *Pseudanabaena* PCC 7403: both filament types have a diameter of 2 μm. However, the similarity ends there, because *Pseudanabaena* possesses marked indentations at the cell division planes but *E. filiformis* does not.

The three variants of *Gunflintia* in Figure 11 have correlation lengths in the 300–700 μm range for populations with apparent diameters of 1–4 μm: *G. minuta* lies near the *Geitlerinema* curve and the *L* subgroup of *G. grandis* lies near the *Oscillatoria* curve. Further, *G. minuta* has the largest correlation length and paradoxically the smallest diameter of the *Gunflintia* group. Within modern filaments, one would not expect ξ_{2p} to decrease as the filament diameter increases, yet this would be the case here if these three populations of *Gunflintia* were truly from the same genus and had similar mechanical structures. In other words, the behavior of the correlation lengths suggests that *G. minuta* and *G. grandis* may be members of different genera. This also may be true for the two subpopulations of *G. grandis* that appear in the measured distributions of filament diameter: ξ_{2p} of the *S* and *L* subgroups are very similar, with a mean value of 360 μm for the two populations, and yet ξ_{2p} of the *L* population should be much larger than the *S* population if R^3 or R^4 scaling applies. Of course, this conclusion is subject to the caveat that the filament diameters observed for the microfossils are their native values and were not changed by the fossilization process.

At less than 50 μm, the very short tangent correlation length of the taxon *Halythrix* is much lower than the range found among our selection of modern cyanobacteria. Nevertheless, ξ_{2p} of *Halythrix* is not that far removed from the extrapolated fit to *Oscillatoria* in Figure 11, although the apparent mechanical structures of these two types of filaments are not superficially similar. Such a high degree of flexibility may reflect the loose connectivity between successive cells in *Halythrix* as a sheathless trichome compared to the hollow tube appearance of *E. filiformis* or *Gunflintia*. As the catalog of measured values of ξ_t for modern filamentous cells enlarges, the behavior of *Halythrix* will become better understood.

Lastly, we turn to the 3.23-Ga pyritic replacement filaments. The magnitude of ξ_{2p} determined for these objects is below *Gunflintia* and *E. filiformis* by factors of three or more, although it is still larger than *Halythrix*. However, pyritic replacement filaments are also relatively narrow, and the combination of their width and tangent correlation length is completely consistent with an extrapolation of the empirical description of ξ_2 of *Geitlerinema*, as seen in Figure 11. Addressing the biological origin of these objects, we confirm that their tangent correlation length is less than for modern cyanobacteria, but lies in the expected range if their narrow measured width is not far removed from the native width when the cells were alive.

From the cell length-to-width ratio of modern filaments, we have conjectured that the ξ_2 versus *D* relationship of *Geitlerinema* and *Oscillatoria* may represent soft limits to the achievable range of ξ_2, such that most filaments should have ξ_2 within these two boundaries. Thus, it may be that *G. minuta* and the pyrite filaments represent large cell length-to-width ratios, whereas *G. grandis L* and *Halythrix* have small such ratios. *E. filiformis* would have a length-to-width ratio slightly larger than unity. Realistically, a database with at least triple the number of genera of modern filaments would have to be constructed in order to confirm this conjecture.

The encouraging feature of the ξ_t versus *D* relationship in Figures 10 and 11 is the broad range covered by the data. If the correlation length were described by just a single function of the cell diameter, then little could be learned by measuring ξ_t of microfossils except their possible deviation from the universal behavior of modern cells. However, the fact that ξ_t of modern cells varies by more than an order of magnitude for a given cell diameter argues that the structure of the filament plays a measurable role in determining ξ_t. Consequently, one should be able to

probe the native mechanical properties of microfossils by using ξ_t as a metric.

Although it is not particularly easy to measure, the torsion resistance of a filament also plays a role in its deformation under stress. Analogous to the bending rigidity, the torsional rigidity κ_{tor} is related to the elastic properties and geometry of a filament. As an illustration, the torsional rigidity of a solid cylinder is given by $\kappa_{tor} = \mu\pi R^4/2$, where μ is the shear resistance of the material; this equation can be used to build up expressions for the torsional properties of hollow tubes or inhomogeneous cylinders as was done for the bending resistance. Isotropic materials possess two independent elastic moduli: there are several different representations of these moduli, of which Y and μ are one such pair. Although it would be very satisfying to independently determine both Y and μ of a filamentous microfossil, this is likely to be an even more challenging task than it is for modern filaments, where measurements of μ are scarce.

In the discussion above, we have repeatedly emphasized the importance of the assumption that the width of a microfossil filament is not very different from its width as a living cell. Another caveat to bear in mind is whether the natural curvature of a filament could be accentuated by inhomogeneous crystalization in its environment after death. One could imagine a scenario in which the curvature increased, which in turn would *decrease* the apparent tangent correlation length. Across several taxa with differing flexural rigidities in the same physical environment, all filaments would appear more flexible, although the relative ordering of ξ_t with κ_f would be unchanged. Unfortunately, we have insufficient data to test this idea.

Summary

In this paper, we have introduced the tangent correlation length, ξ_t, as a means of characterizing, comparing, and interpreting the sinuous shapes of filamentous microfossils and algae. Drawing material from new specimens as well as existing collections, tangent correlation functions have been constructed from images of four taxa of filamentous microfossils in the 2-Ga age range, as well as for 3.23-Ga pyritic replacement tracks. Both to provide a database for interpreting these taxa and to test the applicability of correlation lengths in the context of living cells, we have cultured, imaged and analyzed six strains of filamentous cyanobacteria from the Pasteur Culture Collection. Two additional cultured strains did not prove to be amenable to analysis. Within a given genus of the modern cells, the tangent correlation length increases as $D^{3.3\pm1}$ for *Oscillatoria* and $D^{5.1\pm1}$ for *Geitlerinema*, where D is the filament diameter. These results are consistent with the continuum mechanics analysis of the deformation of uniform rods, where the resistance against bending is predicted to rise as D^4 for solid cylinders and D^3 for hollow tubes. With such simple mathematical functions for the relationship between ξ_t and D, our measurements of modern cyanobacteria can be extrapolated further into the domain of filament diameters relevant to microfossils.

We found that the magnitudes of ξ_t for *Gunflintia* and *E. filiformis* microfossils are similar to those for selected species of modern *Geitlerinema* and *Pseudanabaena* with the same diameters. However, this observation does not establish that these microfossil taxa are cyanobacteria, given that ξ_t of eukarytic green algae of the same diameter are also within this range. If the assignment of *G. minuta*, *G. grandis S*, and *G. grandis L* to the genus *Gunflintia* is correct, then they would have the unusual property that their apparent stiffness did not rise with increasing filament diameter. Alternative explanations for this behavior are that these populations are members of different genera, or that the filament diameter changed upon fossilization. The taxon *Halythrix* possesses a tangent correlation length that is well below ξ_t of the modern filaments in our suite of measurements. However, for its diameter, *Halythrix* lies not too far from the extrapolated function describing three species of modern *Oscillatoria*. Lastly, we found that ξ_t of a set of 3.23-Ga pyritic replacement filaments, while also below modern cyanobacteria, is nevertheless consistent with the extrapolated function describing the D-dependence of ξ_2 for *Geitlerinema*.

We have conjectured that *Geitlerinema* and *Oscillatoria* may lie near soft limits for the accessible range of ξ_t as a function of filament width, although ξ_t will have to be measured for a much larger suite of modern filaments to establish this hypothesis. However, it is very encouraging that ξ_t varies as much as it does for a fixed cell diameter: this variation arises from the cell's structure and composition, so systematic measurements of modern cells should be able to correlate some of these characteristics with changes in ξ_t. In turn, the measured correlation lengths of microfossils at known filament width may lead to characterization of their cells' mechanical components before fossilization.

Acknowledgments

The authors wish to thank H. Hofmann and J. Dougherty for many patient discussions and for facilitating access to the microfossil collection at the Geological Survey of Canada in Ottawa. DB is indebted to H. Boal, who helped obtain the Gunflint material reported here. The Physics and Astronomy Department at Michigan State University (MSU) graciously provided laboratory space for completing this project; M. Velbel of MSU's Geological Sciences Department was the source of considerable advice on sample preparation. This work is supported in part by the Natural Sciences and Engineering Research Council of Canada.

Literature Cited

Atlas, R. M. 2004. Handbook of microbiological media. CRC Press, Boca Raton, Fla.

Awramik, S. M., and E. S. Barghoorn. 1977. Gunflint microbiota. Precambrian Research 5:121–142.

Barghoorn, E. S., and J. W. Schopf. 1966. Microorganisms three billion years old from the Precambrian of South Africa. Science 152:758–763.

Barghoorn, E. S., and S. A. Tyler. 1965. Microorganisms from the Gunflint chert. Science 147:563–577.

Boal, D. H. 2002. Mechanics of the cell. Cambridge University Press, Cambridge.

Brasier, M. D., O. R. Green, A. P. Jephcoat, A. K. Kleppe, M. J. Van Kranendonk, J. F. Lindsay, A. Steele, and N. V. Grassineau. 2002. Questioning the evidence for Earth's oldest fossils. Nature 416:76–81.

Buick, R., C. W. Brauhart, P. Morant, J. R. Thornett, J. G. Maniw, N. J. Archibald, M. G. Doepel, I. R. Fletcher, A. L. Pickard, J. B. Smith, M. E. Barley, N. J. McNaughton, and D. I. Groves. 2002. Geochronology and stratigraphic relationships of the Sulphur Springs Group and Strelley Granite: a temporally distinct igneous province in the Archaean Pilbara Craton, Australia. Precambrian Research 114:87–120.

Cloud, P. E., Jr. 1965. Significance of the Gunflint (Precambrian) microflora. Science 148:27–35.

Fralick, P., D. W. Davis, and S. A. Kissin. 2002. The age of the Gunflint Formation, Ontario, Canada: single zircon U-Pb age determinations from reworked volcanic ash. Canadian Journal of Earth Sciences 39:1085–1091.

Furnes, H., N. R. Banerjee, K. Muehlenbachs, H. Staudigel, and M. de Wit. 2004. Early life recorded in Archean pillow lavas. Science 304:578–581.

Golubic, S., and H. J. Hofmann. 1976. Comparison of modern and mid-Precambrian Entophysalidaceae (Cyanophyta) in stromatolitic algal mats: cell division and degradation. Journal of Paleontology 50:1074–1082.

Hofmann, H. J. 1975. Stratiform, Precambrian stromatolites, Belcher Islands, Canada: relations between silicified microfossils and microstructure. American Journal of Science 275:1121–1132.

———. 1976. Precambrian microflora, Belcher Islands, Canada: significance and systematics. Journal of Paleontology 50:1040–1073.

Knoll, A. H., and E. S. Barghoorn. 1974. Ambient pyrite in Precambrian chert: new evidence and a theory. Proceedings of the National Academy of Sciences USA 71:2329–2331.

Knoll, A. H., E. S. Barghoorn, and S. M. Awramik. 1978. New microorganisms from the Aphebian Gunflint Iron Formation, Ontario. Journal of Paleontology 52:976–992.

Rasmussen, B. 2000. Filamentous microfossils in a 3.235-million-year-old volcanogenic massive sulphide deposit. Nature 405:676–679.

Rippka, R. 1988. Isolation and purification of cyanobacteria. Methods in Enzymology 167:3–27.

Schopf, J. W. 1968. Microflora of the Bitter Springs Formation, Late Precambrian, central Australia. Journal of Paleontology 42:651–688.

———. 1993. Microfossils of the Early Archean Apex chert: new evidence of the antiquity of life. Science 260:640–646.

Schopf, J. W., and B. M. Packer. 1987. Early Archean (3.3-billion to 3.5 billion-year-old) microfossils from Warrawoona Group, Australia. Science 237:70–73.

Tyler, S. A., and E. S. Barghoorn. 1963. Ambient pyrite grains in Precambrian cherts. American Journal of Science 261:424–432.

Vearncombe, S., M. E. Barley, D. I. Groves, N. J. McNaughton, E. J. Mikucki, and J. R. Vearncombe. 1995. 3.26 Ga black smoker-type mineralization in the Strelley Belt, Pilbara Craton, Western Australia. Journal of the Geological Society, London 152:587–590.

Walsh, M. M., and D. R. Lowe. 1985. Filamentous microfossils from the 3,500 Myr-old Onverwacht Group, Barberton Mountain Land, South Africa. Nature 314:530–532.

Appendix

For the interested reader, we now describe in slightly more mathematical detail the origin of several expressions that were introduced without proof in the main text. Our starting point is the well-known result from statistics that the end-to-end displacement $\mathbf{r}_{ee}$ for an ensemble of random walks each with N steps of equal length a is governed by

$$\langle r_{ee}{}^2 \rangle = Na^2 = L_3 a, \tag{A1}$$

where $<\ldots>$ denotes the usual ensemble average and $L_3 = Na$ is the contour length of the walk, which we take to be in three dimensions (although equation (A1) is of general validity). The walks are random in the sense that the direction of each successive step is independent of the neighboring steps. If a walk had some ''stiffness'' to it, say each new step could change direction by not more than 90°, then the average end-to-end

distance would be larger. Such behavior is can be accommodated in the more general form of equation (A1):

$$\langle r_{ee}{}^2 \rangle = 2L_c\xi_t, \tag{A2}$$

which arises when the tangent correlation function for the walks obeys equation (2), where ξ_t is the tangent correlation length (see Boal 2002). Comparing equations (A1) and (A2), one finds $\xi_t = a/2$ for a random walk.

When a three-dimensional walk of fixed step length a is projected onto a two-dimensional plane, the mean projected step length is reduced to $a_{2p} = a\langle\sin\theta\rangle = a\int_o^{\pi/2} \sin^2\theta\, d\theta = (\pi/4)a$, where θ is the angle between the z-axis and the direction of the step in the walk. The subscript 2p denotes the projected value; note that $\langle a^2\rangle_{2p} = (2/3)a^2$. In terms of a_{2p}, the projected contour length is $L_{2p} = Na_{2p} = (\pi/4)Na$. Thus, the mean square value of the projected end-to-end displacement is

$$\langle r_{ee}{}^2\rangle_{2p} = N\langle a^2\rangle_{2p} = (8/3\pi)L_{2p}a, \tag{A3}$$

from which equation (3), $\xi_3 = (3\pi/8)\ \xi_{2p}$, is obtained via the definition $\langle r_{ee}{}^2\rangle_{2p} \equiv 2L_{2p}\xi_{2p}$.

These first few equations are general results for sinuous curves and make no specific reference to a physical system such as string or tube, even though ξ_t of a physical system implicitly depends on its resistance to bending, characterized by its flexural rigidity κ_f. Physical systems like rods and tubes can be gently bent at an energetic cost that is proportional to the square of the rate of change of the tangent vector along rod, $\partial\mathbf{t}/\partial s$:

$$[\textit{deformation energy per unit length}] = (\kappa_f/2)\ (\partial\mathbf{t}/\partial s)^2. \tag{A4}$$

For rods with uniform composition and fixed cross-sectional shape, the flexural rigidity κ_f in equation (A4) is given by

$$\kappa_f = YI \tag{A5}$$

(see Boal 2002 and references therein), where Y is the Young's modulus of the material from which the rod is made, and I is the moment of inertia of the cross-section of the rod,

$$I = \int x^2\, dA. \tag{A6}$$

In equation (A6), the area-weighted integration dA is over the distance x from an axis in the plane of the cross-section; the bending motion of the rod is around this axis. For a uniform solid rod of circular cross-section with radius R, equation (A6) yields $I = \pi R^4/4$. For a hollow tube with a wall thickness of t and outer radius R, the moment of inertia of the cross-section is $I = \pi[R^4 - (R\text{-}t)^4]/4$ which can be expanded as $I = \pi R^3 t - (3\pi/2)R^2t^2 + \ldots$. If the thickness of the tube wall is small compared to its radius ($t \ll R$), only the leading order term in the expression for I need be kept, such that $I = \pi R^3 t$. For a rod in thermal equilibrium in a quiescent medium at temperature T, it can be shown that ξ_t is directly proportional to κ_f and obeys $\xi_t = \kappa_f/k_BT$, where k_B is Boltzmann's constant.